Hindawi
Journal of Sensors
Volume 2018, Article ID 5847081, 14 pages
https://doi.org/10.1155/2018/5847081

Research Article

A Novel Weak Signal Detection Method of Electromagnetic LWD Based on a Duffing Oscillator

Aiping Wu,[1,2] Saleh M. Mwachaka,[1,3] Yanliang Pei,[2,4] and Qingqing Fu[1]

[1]*National Demonstration Center for Experimental Electrical & Electronical Education, Yangtze University, Jingzhou, Hubei 434023, China*
[2]*Laboratory for Marine Geology, Qingdao National Laboratory for Marine Science and Technology, Qingdao 266061, China*
[3]*Faculty of Computing, Information Systems and Mathematics, Institute of Finance Management, P.O. Box 3918, Dar es Salaam, Tanzania*
[4]*Key Laboratory of Marine Sedimentology and Environmental Geology, First Institute of Oceanography, SOA, Qingdao 266061, China*

Correspondence should be addressed to Qingqing Fu; jpufqq@yangtzeu.edu.cn

Received 29 January 2018; Revised 27 March 2018; Accepted 12 April 2018; Published 21 June 2018

Academic Editor: Hyung-Sup Jung

The logging while drilling (LWD) electromagnetic weak signal detection model of a Duffing oscillator based on a one-dimensional nonlinear oscillator is established. The influences of noise on Duffing oscillator dynamic behavior of periodic driving force are discussed and evaluate the oscillator weak signal detection mechanism based on a phase change trajectory diagram. The improved Duffing oscillator is designed and applied to detect the electromagnetic logging signal resistivity at the drill bit using the time-scale transformation method. The simulation results show that the nonlinear dynamic characteristics of the Duffing oscillator are very noticeable, the Duffing circuit is very sensitive to detect the tested signal, and it has a reasonable level of immunity to noise. The smaller the amplitude of the tested signal, the more sensitive the circuit is to the signal, the better the antinoise system performance, and the lower the signal-to-noise ratio (SNR).

1. Introduction

During the logging while drilling (LWD) process, the drilling environments pose extreme challenges on the course of data detection, consequently changing the drilling signal properties and disrupting the surface signal detection, extraction, and interpretation. Accurate drilling information determines the correct directional drilling variables and geological formation from the wellbore to improve drilling efficiency [1, 2]. Drilling signal pulses experience unpredictable and complex adjustable signal impairments caused by friction between drill bit and stratum formation, drill string vibration noises, signal attenuation and drilling fluid circulations, high temperature, and high pressure of the downhole environment [3–6]. The impact leads to profound signal disruption and noise sources at the surface measurement system, resulting in surface signal detection complexity. On the other hand, the penetration of the drilling fluid causes the formation of mud cake, flushing zone, and transition zone along the radial direction of the borehole wall, and finally the undisturbed formation contains stratum information transmitted as signals to be detected by the surface receiver system [7, 8]. Greater well depths along the radial LWD equipment direction require depth drilling instruments which increase the signal transmission distances, consequently resulting in extremely weaker surface-detected signals. Therefore, the study of weak signal detection in the presence of strong noise is vital to improve the detection performance of logging tools.

Based on the chaotic nonlinear theory, this paper studies the weak signal detection method of a Duffing oscillator with azimuth electromagnetic wave logging resistivity. Using a one-dimensional nonlinear oscillator model, the Duffing oscillator detection model is established. The dynamic simulation analysis was carried out to study the influence of noise

on the Duffing oscillator movement. The Duffing oscillator circuit is extended to improve its application into electromagnetic resistivity LWD signal detection based on the time-scale transformation technique. The paper discusses the use of circuit simulation to realize physical Duffing oscillator performance on the azimuth electromagnetic logging weak signal detections.

The rest of the paper proceeds as follows: Section 2 discusses the weak signal detection techniques, Section 3 describes the general and improved Duffing oscillator circuit and the influence of noise on Duffing oscillator movement, Section 4 discusses the simulation results of various Duffing oscillator phase state performances, and Section 5 discusses the paper summary while Section 6 draws the paper conclusion.

2. Weak Signal Detection Techniques

Modern signal processing techniques for weak signal detection methods, principally, apply the conventional methods based on time- and frequency-domain techniques. Conventional time-domain weak signal detection methods mostly implement the correlation detection method [9] and sampling integral and time-domain averaging method [10, 11], such as those using the locking amplifier and sampling integrator. Frequency-domain methods are based on the signal power spectrum analysis [12] but are more suitable for weak periodic signal detections. Other weak signal detection methods deploy wavelet analysis [13, 14], high-order spectrum analysis [15, 16], Hilbert-Huang transform [17], and artificial neural network [18]. However, in the wavelet analysis, the selection of the wavelet base function and the scale range are very complex and lack the general method. High-order spectrum statistics analysis is an effective stochastic signal analysis tool that can effectively solve the objective non-Gaussian and nonlinear problems.

Initially, locally optimum detectors using the Neyman-Pearson approach performance criterion based on the additive noise model have been deployed to provide correct weak signal detection for the fixed value probability of false detection or false alarm [19]. The design used known signal sequence in which the observations represent either noise only or a signal with additive noise and specific sample size signal value. The additive noise models used approximation of actual circumstances and are not convenient to implement under certain consideration. Nonadditive noise models are necessary and cannot be ignored in multiplicative and signal-dependent noise communications, acoustics, and image processing applications [20]. The level of the contribution of higher-order statistics or of nonlinearity is not negligible. The nonadditive noise model to produce realistic and reasonable weak signal detection approximations has to be devoted to overcome the significant penalty which results from using the incorrect (additive noise) model. Most modem signal detectors based on statistical hypothesis testing assume the digital domain processing the useful and inevitable quantizer-detector model in modem signal detection problems.

Signal processing of weak signal detection using narrowband high-order statistics attained a certain effect in the context of Gaussian noise but was only capable to inhibit white noise and Gaussian noise and took very large amount of calculations [15]. Neural network analysis uses an algorithmic mathematical model that simulates the neural structure of biological organisms to carry out distributed parallel information processing. By adjusting the interconnection relationship between large numbers of nodes, the neural network can be used to achieve information processing. Signal detection based on the neural network algorithm imposes setting the weight and critical values that need a lot of sample training. In case the noise type or magnitude changes, the neural network must be retrained; this limits the application of the neural network in the weak signal detection.

The traditional weak signal detection method estimates the noise signals to be the interfering signal whereby the original weak signal detection is achieved by noise suppression techniques. However, during noise suppressions, inevitably, useful signal is distorted, as this is a detrimental detection technique. In this situation, weak signal detection researchers began to carry out study on techniques to detect weak signal without destroying the useful signal in the low SNR conditions based on utilizing the noise rather than on suppressing it. In recent years, research and development of nonlinear science has provided novel weak signal detection techniques.

3. Proposed Method

3.1. Duffing Oscillator Model. The vibration law of the one-dimensional periodic driving force vibration system can be expressed mathematically as a differential equation shown by

$$\ddot{x} + \phi(x, \dot{x}) + f(x) = E(t), \tag{1}$$

where "·" and "··" represent the first and second derivative of time t, respectively; $\ddot{x}$, $\dot{x}$, and x represent the acceleration, velocity, and displacement of the particle, respectively; $\phi(x, \dot{x})$ represents the damping force; $f(x)$ represents the resilience; and $E(t)$ represents the periodic driving force.

In the study of engineering kinetic technology, the calculation and analysis of nonlinear vibration characteristics describe the Duffing nonlinear oscillator with the cubic derivative term for the spring effect of mechanical complications. The proposed standardized Duffing equation becomes

$$\ddot{x} + k\dot{x} + \alpha x + \beta x^3 = \gamma \cos(\omega t), \tag{2}$$

where k represents the damping ratio coefficient, α and β are the linear and nonlinear stiffness coefficients, respectively, of the spring, and γ represents the amplitude of the periodic driving force.

On this basis, Moon and Holmes modify the Duffing equation to describe the support beam forced vibration in the inhomogeneous (nonuniform) magnetic field of the two permanent magnets, named as Duffing-Holmes described by

$$\ddot{x} + k\dot{x} - x + x^3 = \gamma \cos(\omega t). \tag{3}$$

From (3), the magnitude of the damping ratio coefficient, k, and the amplitude of the periodic driving force, γ, are variable parameters, while $-x + x^3$ is defined as the nonlinear restoring force and $\gamma \cos \omega t$ named as the external periodic dynamic force. The Duffing equation has strong dynamic behavior, with noticeable nonlinear dynamic characteristics, creating one of the typical nonlinear dynamic system behavior applications.

In order to facilitate the analysis of the Duffing equation and achieve the purpose of reducing the order, (3) can be expressed as the differential equation:

$$\begin{aligned} \dot{x} &= y, \\ \dot{y} &= -ky + x - x^3 + \gamma \cos(\omega t). \end{aligned} \tag{4}$$

3.2. The Influence of Noise on Duffing Oscillator Movement. Due to the complex downhole conditions, the logging signal transmission process is disturbed by all kinds of noises which causes the surface-collected signal to contain many signal noises that weaken the amplitude and hence challenge the signal detection. Assuming that $n(t)$ is the background noise in the detection process with zero expectation and the variance is σ^2, then, the solution $x(t)$ of (3) in the critical state has a small change, $\Delta x(t)$, to the detection system output $x(t)$. Therefore, the system detection equation can be expressed as:

$$(\ddot{x} + \Delta\ddot{x}) + k(\dot{x} + \Delta\dot{x}) - (x + \Delta x) + (x + \Delta x)^3 = \gamma \cos(\omega t) + n(t). \tag{5}$$

Subtracting (5) from (3), the new generated equation becomes

$$\Delta\ddot{x} + k\Delta\dot{x} - \Delta x + 3x^2\Delta x + 3x(\Delta x)^2 + (\Delta x)^3 = n(t). \tag{6}$$

The variable change, $\Delta x(t)$, is very small compared to the system output detection $x(t)$. Therefore, by ignoring the high order of $\Delta x(t)$, the vector differential equation changes to

$$\Delta\dot{\mathbf{X}}(t) = \mathbf{H}(t)\Delta\mathbf{X}(t) + \mathbf{N}(t). \tag{7}$$

Each vector in the differential equation (7) can individually be expressed as

$$\begin{aligned} \Delta\mathbf{X}(t) &= \begin{pmatrix} \Delta x(t) \\ \Delta\dot{x}(t) \end{pmatrix}, \\ \mathbf{H}(t) &= \begin{pmatrix} 0 & 1 \\ 1 - 3x^2(t) & -k \end{pmatrix}, \\ \mathbf{N}(t) &= \begin{pmatrix} 0 \\ n(t) \end{pmatrix}. \end{aligned} \tag{8}$$

According to the solution existence and uniqueness theorem, the vector differential equation (7) has a unique solution that satisfies an initial condition which can be expressed as

$$\Delta\mathbf{X}(t) = \mathbf{\Phi}(t, t_0)\Delta\mathbf{X}_0 + \int_{t_0}^{t} \mathbf{\Phi}(t, u)\mathbf{N}(u)du. \tag{9}$$

Due to the performance analysis of the system at a steady state from (9), $\mathbf{\Phi}$ is the state matrix of the system. The first item is a transient solution, so the phase trajectory decays exponentially to 0 at time, t, and the second item (statistical characteristic analysis) provides the expectation (mean) expressed as

$$E[\Delta\mathbf{X}(t)] = \int_{t_0}^{t} \mathbf{\Phi}(t, u)E[\mathbf{N}(u)]du = 0. \tag{10}$$

The matrix variance can further be simplified and expressed as

$$\begin{aligned} \mathbf{R}_{\Delta x}(t, t) &= \int_{-\infty}^{t}\int_{-\infty}^{t} \mathbf{\Phi}(t, u)\mathbf{R}[N(u), N(v)]\mathbf{\Phi}^T(t, u)dudv \\ &= \int_{-\infty}^{t}\int_{-\infty}^{t} \mathbf{\Phi}(t, u)E\left[\begin{pmatrix} 0 \\ n(u) \end{pmatrix}(0, n(v))\right]\mathbf{\Phi}^T(t, u)dudv \\ &= \int_{-\infty}^{t}\int_{-\infty}^{t} \mathbf{\Phi}(t, u)\begin{pmatrix} 0 & 0 \\ 0 & \sigma^2\delta(u - v) \end{pmatrix}\mathbf{\Phi}^T(t, u)dudv \\ &= \sigma^2\int_{-\infty}^{t} \mathbf{\Phi}(t, u)\begin{pmatrix} 0 & 0 \\ 0 & 1 \end{pmatrix}\mathbf{\Phi}^T(t, u)du. \end{aligned} \tag{11}$$

The dynamic characteristics of the Duffing oscillator analysis show that as long as the mathematical expectation of the noise is zero, the noise has no decisive change. This concludes that the noise does not fundamentally change the phase of the system but only makes the phase trajectory of the system rough; the roughness is determined by the variance of the disturbance, but the overall system mean is zero. Additionally, since the noise distribution problem in the above analysis process is not principally limited, the Duffing oscillator has a good immune performance for any randomly distributed stochastic noise.

3.3. Improved Duffing Oscillator. The traditional Duffing equation applies only to low frequency ranges while electromagnetic logging coil waves use high frequencies such as 2 MHz, 1 MHz, and 400 kHz. In order to apply the advanced weak signal detection technique based on electromagnetic LWD signal data acquisition systems, the improved dynamic equation that uses phase trajectory time-scale transformation to detect high-frequency signal can be expressed as

$$\ddot{x}(t) + k\dot{x}(t) - x(t) + x^3(t) = \gamma \cos(\omega t). \tag{12}$$

Assuming $t = \omega\tau$, computing $x(t)$ becomes $x(t) = x(\omega\tau) = x_\xi(\tau)$.

$$\dot{x}(t) = \frac{dx(t)}{dt} = \frac{1}{\omega}\frac{dx_\xi(\tau)}{d\tau} = \frac{1}{\omega}\dot{x}(\tau). \tag{13}$$

Equation (13) can further be simplified to

$$\ddot{x}(t) = \frac{1}{\omega^2}\frac{d^2x_\xi(\tau)}{d\tau^2} = \frac{1}{\omega^2}\ddot{x}(\tau). \tag{14}$$

Substituting (13) and (14) into (12), the new simplified equation changes to

$$\frac{1}{\omega^2}\ddot{x}_\xi(\tau) + \frac{k}{\omega}\dot{x}_\xi(\tau) - x_\xi(\tau) + x_\xi^3(\tau) = \gamma \cos(\omega\tau). \quad (15)$$

In order to facilitate the analysis of the equation, while achieving the purpose of reducing the order, (15) can be expressed by the differential state equations as follows:

$$\begin{aligned} \dot{x} &= \omega y, \\ \dot{y} &= \omega\left[-ky + x - x^3 + \gamma \cos(\omega t)\right]. \end{aligned} \quad (16)$$

3.4. Response Signal Amplitude Detection. The method of detecting the amplitude of the signal using the Duffing oscillator uses system characteristics sensitive to the signal parameter to be tested and immune to noise signal. The basic detection idea is to set the frequency of the internal power (driving force) signal to be the same as the frequency of the signal to be measured and then adjust the amplitude $r1$ of the internal driving force signal to make the system in chaotic critical state. The applied periodic signal to the Duffing oscillator system is used as the source signal and the internal driving force which must be in the same frequency and phase as the internal power signal. Increase the driving force magnitude until the system changes from the chaotic state into the large-scale periodic state and then gradually reduce the amplitude of the internal power until the system enters again into the chaotic critical state, and record the internal driving force amplitude at this time, $r2$. The amplitude of the signal to be measured and detected, $r0$, is computed as the amplitude difference between the magnitudes of the internal driving force when the system is in the critical state and when it enters the chaotic state from the large periodic state, that is, $r0 = r1 - r2$.

By automatically adjusting the amplitude of the internal driving force and identifying the phase, the signal amplitude can be detected and determined by the block diagram shown in Figure 1. The modified Duffing-Holmes equation is used to simulate the model; the vibrator (oscillator) movement state is related to the magnitude of the damping coefficient ratio, k, and the amplitude of the excitation force, γ, of the periodic driving force. Any changes or disturbances into these parameters can obviously change the output phase of the system. The damping coefficient and the power of the disturbance can be observed during signal detection. The signal is detected by consistent disturbance of the measured signal damping coefficient ratio and the amplitude of the power signal amplitude $r1$ in a chaotic critical state.

The damping coefficient ratio, γ, can be used to calculate the damping coefficient of the Duffing oscillator, and the detection model becomes

$$\ddot{x} + k[1 + d(t)]\dot{x} - x + x^3 = \gamma \cos(\omega t). \quad (17)$$

where $d(t)$ is the signal to be measured with background noise and is in phase and smaller than the amplitude of the internal power signal. Before adding the signal, the damping coefficient ratio is adjusted to make the Duffing oscillator system in the chaotic critical state, and the critical damping coefficient is expressed as k_c. The damping coefficient ratio of the vibrator is changed to $k[1 + d(t)]$, which changes with the adjustment of the signal to be measured. In the condition that the amplitude of the oscillator driving signal is constant, the decrease of the system damping coefficient ratio reduces the system from the chaotic state into the periodic state, so as to achieve signal detection.

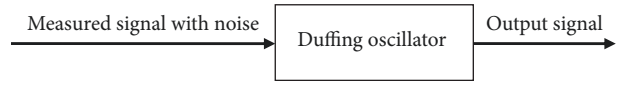

Figure 1: Duffing oscillator detection system.

The system disturbance mode is to use the perturbation of the signal to be measured as the internal driving force to the Duffing oscillator. The detection model becomes

$$\ddot{x} + k\dot{x} - x + x^3 = \gamma \cos(\omega t) + d(t). \quad (18)$$

Before adding the signal, the internal driving force damping ratio amplitude is adjusted first until the oscillator is in the chaotic critical state. Then, the measured signal, $d(t)$, is applied to the oscillator system, and the amplitude of the periodic power signal is changed. Based on the previous analysis, certain noise intensity cannot cause phase properties to change but only partially changes the width of the phase trajectory diagram. In order to achieve weak signal detection submerged into noise signals even with very small signal amplitude, the system must transit rapidly from the chaotic to large-scale periodic state as time changes.

On a serious note, the use of this method to achieve signal detection requires the signal to be measured and the internal driving force signal to have the same frequency and phase. For the known periodic signal frequency to be measured, to generate the same frequency as that of the driving force signal is relatively easy, but for the unknown signal, you must first determine the frequency of the measured signal. Since the excitation frequency of the electromagnetic LWD transmitter coil is controlled by the microprocessor microcontroller unit (MCU), the frequency of the induced signal on the receiving coil can be determined at a specific excitation frequency. The Duffing oscillator can be set according to the excitation frequency of the transmitting coil to detect the electromagnetic logging response signal and the driving force signal frequency.

3.5. Improved Duffing Oscillator Circuit

3.5.1. Fundamental Principle. Basing on the traditional Duffing oscillator, the dynamic equation applied to the detection of high-frequency weak signal using time-scale transformation can be expressed as follows:

$$\begin{aligned} \dot{x} &= \omega y, \\ \dot{y} &= \omega\left[-ky + x - x^3 + \gamma \cos(\omega t)\right]. \end{aligned} \quad (19)$$

From the analogue circuit implementation, (19) can be expressed as an integral form as

$$\begin{aligned} x &= \int \omega y dt + C_1 = \omega \int y dt + C_1, \\ y &= \int \omega \left[-ky + x - x^3 + \gamma \cos(\omega t)\right] dt + C_2 \\ &= \omega \int \left[-ky + x - x^3 + \gamma \cos(\omega t)\right] dt + C_2. \end{aligned} \tag{20}$$

From (20), the damping coefficient ratio, k, is set to 0.5, while C_1 and C_2 are the integral constants. Considering the initial conditions, let x and y initial values be set to 0 and then $C_1 = C_2 = 0$.

From the analogue electronic analysis, the integral circuit used to achieve the integrated operation is an inverting integral circuit (Figure 2). According to the characteristics of the ideal op-amp, the relationship of the output voltage and the input voltage is as follows:

$$U_o = -\frac{1}{RC} \int U_i dt. \tag{21}$$

The inverting integral circuit (Figure 2) represents (21), and the derived Duffing equation (20) can be implemented as an integral circuit above, except that the integral coefficient and the circuit structure are different.

The transmitting coil excitation frequency is 2 MHz, equivalent to an angular frequency, $\omega = 2\pi^* 2^* 10^6$, which is the Duffing oscillator circuit frequency designed.

Since the power supply voltage, V_{CC}, of the circuit is limited and the excitation frequency is very high, if the signal is multiplied by (20), the circuit will be saturated instantaneously and the output voltage will be maintained near the power supply voltage. In order to avoid this problem, the design uses the first integral and then takes a factor, so that the circuit can achieve a high-frequency signal detection. The block diagram of the Duffing circuit according to (20) is shown in Figure 3.

The output signal, y, is $-(1/K_1)\int y dt$ passed through inverting integrator 1 and changes to $(K_2/K_1)\int y dt$ when passed through inverting amplifier 1. In contrast to (20), the output of inverting amplifier 1 is x when $K_2/K_1 = \omega$. The x^3 variable realized by the multiplier changes to $-x^3$ when passed through inverting amplifier 3. The output of inverting amplifier 2 is $-0.5y$ and adder 1 is used to obtain the signal $-0.5y - x^3$ while the output of adder 2 is $-0.5y + x - x^3 + \gamma \cos \omega t$, denoted as $m(t)$. The output signal $m(t)$ changes to $-(1/K_3)\int m(t)dt$ when passed through inverting integrator 2 and further changes to $-(K_4/K_3)\int m(t)dt$ after inverting amplifier 4. If this output is compared to (20), the output of inverting amplifier 4 is y when $K_4/K_3 = \omega$. Therefore, the Duffing oscillator equation can be realized by designing the amplifier circuit and later integrating it.

3.5.2. Duffing Oscillator Circuit Design. According to the circuit design principles of Figure 3, the Duffing equation can be realized by the use of the integrator, amplifier, and adder. The signal detection (20) can be realized when the integral coefficient and system gain satisfy certain assumptions. The integral coefficient and the gain will be determined by the circuit design parameters.

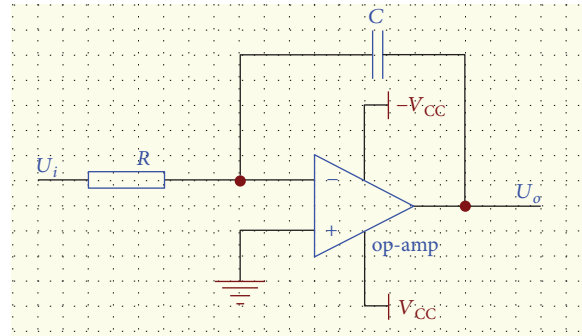

Figure 2: Typical inverting integral circuit.

Taking into account the gain bandwidth and other performance issues, the appropriate closed-loop gain of the single-stage op-amp must be less than 100. To simplify the circuit design parameters, assume that the inverting amplifier 2 gain, K_2, is 12.56 which can be achieved by the precision potentiometer of 20 kΩ and a resistor of 1 kΩ. The proportional coefficient of inverting integrator 2 is $K_1 = 10^{-6}$ for $RC = 10^{-6}$; then, the resistance is 1 kΩ and the capacitance is 1 nF. Since K_3 and K_4 satisfy the same relationship as K_1 and K_2, the parameters of inverting integrator 2 and inverting amplifier 4 will be the same as those of inverting integrator 1 and inverting amplifier 1. Adder 1 and adder 2 do not have multiple gains but have the unit scaling factor; thus, the inverting resistance and feedback resistance are equal with a 10 kΩ value. Inverting amplifier 2 has a gain of 0.5, and the operational amplifier inverting resistor is twice the feedback resistor, with 20 kΩ and 10 kΩ values, respectively. The gain of inverting amplifier 3 is unit, and the operational amplifier inverting resistor is equal to the feedback resistor, both with 10 kΩ values.

4. Result Discussions

4.1. System Phase State. The Duffing oscillator system output response is affected by the change in the damping ratio coefficient, k, the amplitude, γ, and the frequency, ω, of the periodic driving force signal. In order to study the influence of these parameters on the system phase transition, the initial values of the damping ratio and frequency are kept constant while changing the amplitude of the driving force and observing the system phase trajectory variations. The horizontal axis and the vertical axis form the phase curve on the x-y plane. The system phase trajectory is used to describe the system phase state.

The Duffing oscillator numerical simulation model based on MATLAB Simulink from (4) is shown in Figure 4, initially without the influence of noise sources. The system damping ratio coefficient, $k = 0.5$, driving force frequency, $\omega = 1$ rad/s, and the initial values are set to $(x(t), \dot{x}(t)) = (0, 0)$.

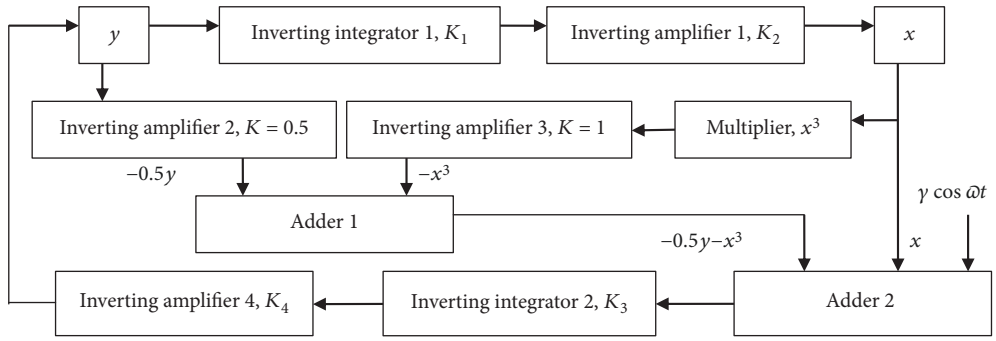

Figure 3: Duffing oscillator circuit block diagram.

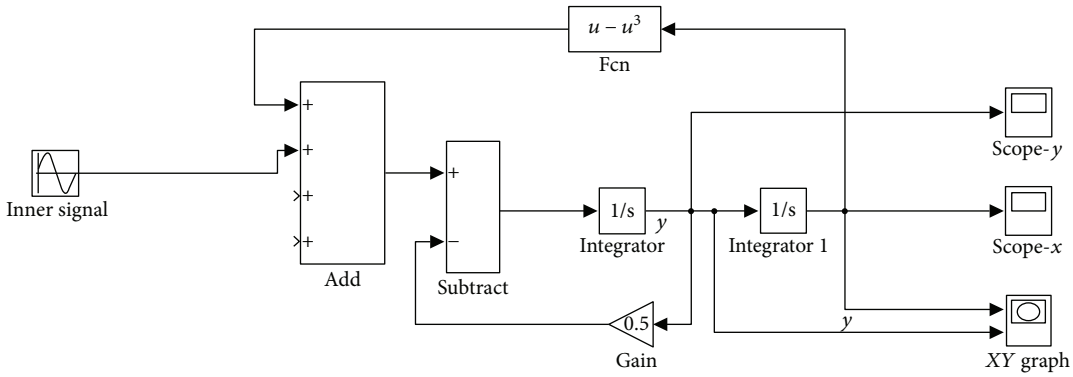

Figure 4: Duffing oscillator model schematic diagram.

The amplitude of the driving force γ increases from 0 to a certain value when the system behaves as an attractor, and the variables x and y eventually stabilize with time t. The phase trajectory diagram oscillates periodically between the equilibrium points as shown in Figure 5(a). When the amplitude γ increases to 0.38, the system phase trajectory is the homoclinic orbit (Figure 5(b)), and the variables x and y fluctuate between 1 and 0, respectively. As the amplitude continues to increase, the variable x fluctuates between values 1 and −1 and the system behaves as a bifurcation, as shown in Figure 5(c). Further, when the amplitude increases but below 0.826, the system enters the chaotic state (Figure 5(d)); when the amplitude increases to reach 0.826, the system enters the critical state where the variables x and y fluctuate between 0 and the volatility value (greater than 1), as shown in Figure 5(e). When the amplitude, γ, exceeds the critical value to 0.8261, the variables x and y exceed the regular large fluctuations between 1 and −1, and the system enters the large-scale periodic orbital state and the phase trajectory is no longer chaotic but repeats along a certain fixed orbit, shown in Figure 5(f).

4.2. The Influence of Noise on Critical and Periodic States

4.2.1. Critical State. The Duffing oscillator numerical simulation model using MATLAB Simulink application to study the influence of noise on the system in the critical state is shown in Figure 6. The damping coefficient of the system is $k = 0.5$. The driving force signal is generated by the inner signal with the frequency, $\omega = 1$ rad/s, having the same frequency and phase with the generated signal while the system initial values are set to $(x(t), \dot{x}(t)) = (0, 0)$.

Initially adjust the system's periodic driving force amplitude, $\gamma = 0.8260$, where the system is in the critical state as shown in the phase diagram (Figure 7(a)). On the same condition, add the white Gaussian noise and gradually increase the noise power. The phase trajectory diagram observed in Figures 7(b)–7(d) shows that the system is still in the chaotic state. When the noise power increase is small, the phase trajectory of the system is relatively smooth indicating that the phase state does not change due to the small increase of the noise power. With the further increase of the noise power, the phase trajectory becomes rough and glitches appear. The simulation results show that the Duffing oscillator in the chaotic critical state has good noise immunity in the presence of certain intensity background noises.

Based on the Figure 6 input signals, the sinusoidal noise signal with 10 mV amplitude is added and monitor the phase trajectory diagram change characteristics corresponding to signal-to-noise ratios (SNR) −3 dB, −13 dB, −16 dB, and −18 dB, shown in Figures 7(e)–7(h), respectively. The addition of the signal to be measured (tested) changes the fundamental system phase state diagram from the chaotic critical state to the large-scale periodic state. When the noise power is small, the system phase trajectory diagram is relatively smooth, and as the noise power increases, the phase

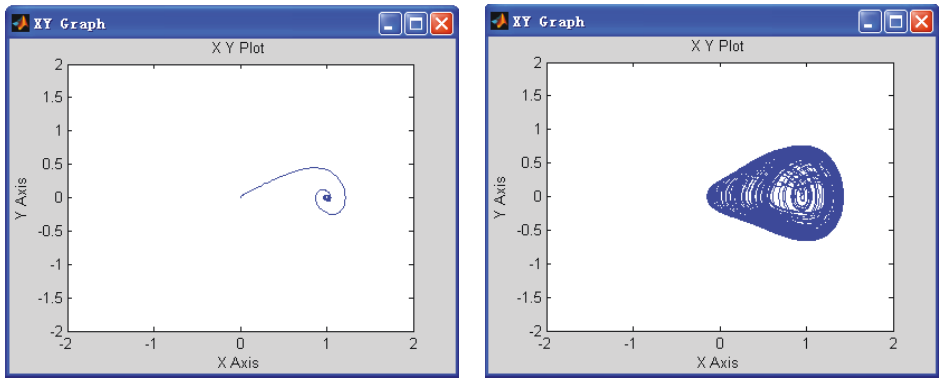

(a) System phase trajectory diagram ($\gamma = 0.03$)

(b) Homoclinic orbit map ($\gamma = 0.38$)

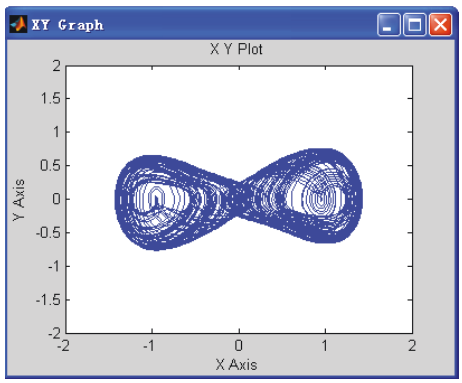

(c) System bifurcation diagram ($\gamma = 0.385$)

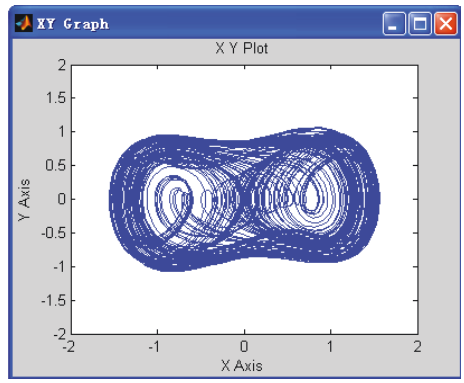

(d) System chaotic diagram ($\gamma = 0.68$)

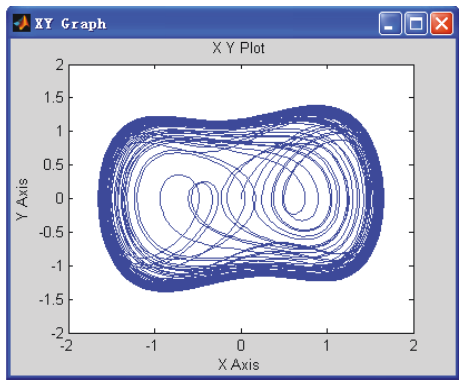

(e) System critical chaotic state ($\gamma = 0.8260$)

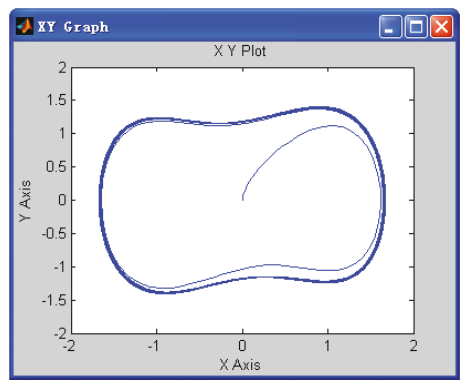

(f) System periodic state ($\gamma = 0.8261$)

Figure 5: Duffing oscillator state diagram.

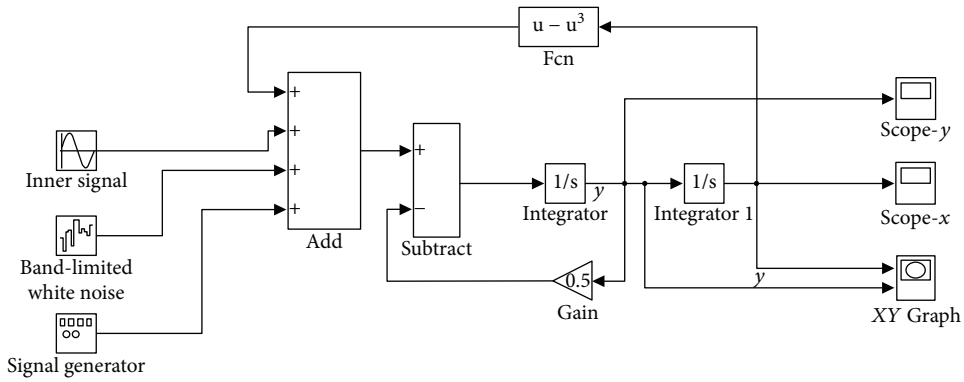

Figure 6: Schematic diagram of the Duffing oscillator with a noise source.

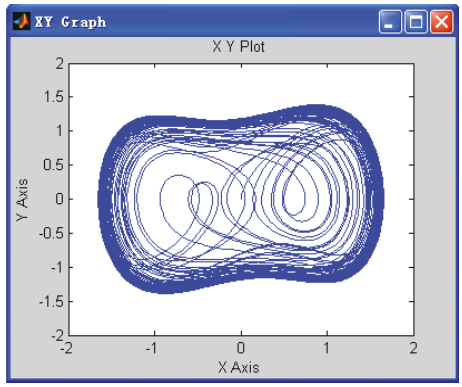

(a) No noise ($r = 0.8260$)

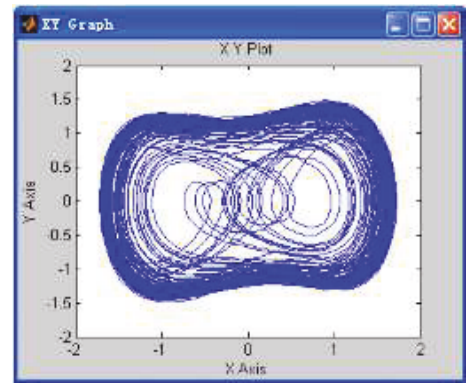

(b) Power = 0.1 mW ($\gamma = 0.8260$)

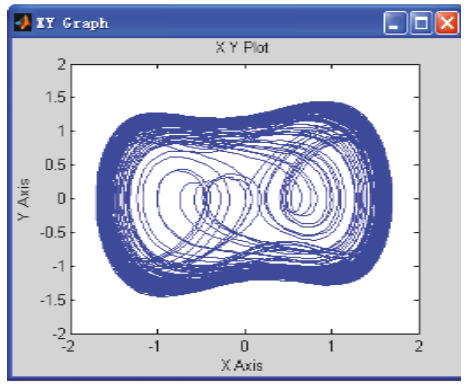

(c) Noise power = 0.5 mW ($\gamma = 0.8260$)

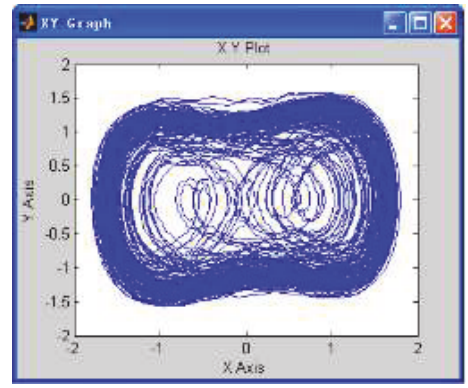

(d) Noise power = 10 mW ($\gamma = 0.8260$)

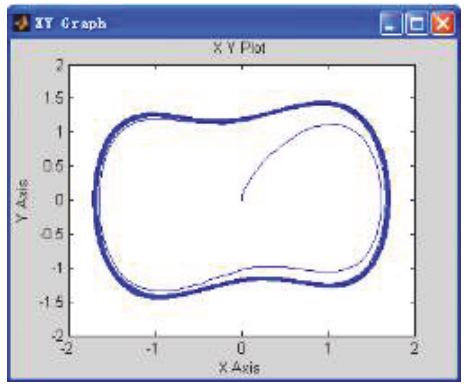

(e) Noise power = 0.1 mW + test signal

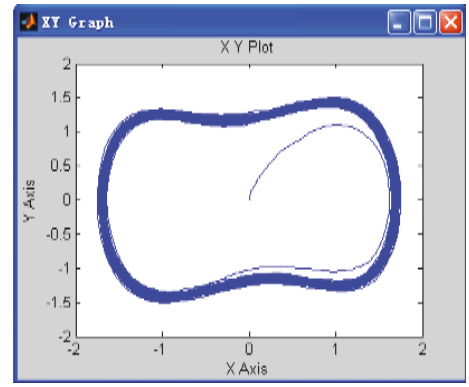

(f) Noise power = 1 mW + test signal

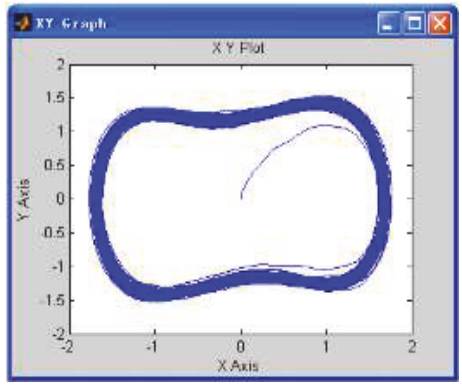

(g) Noise power = 2 mW + test signal

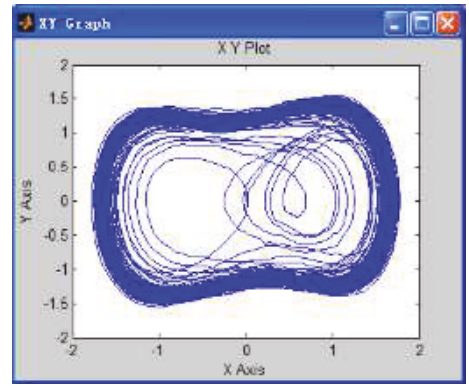

(h) Noise power = 2.8 mW + test signal

Figure 7: System phase trajectory state with different SNR.

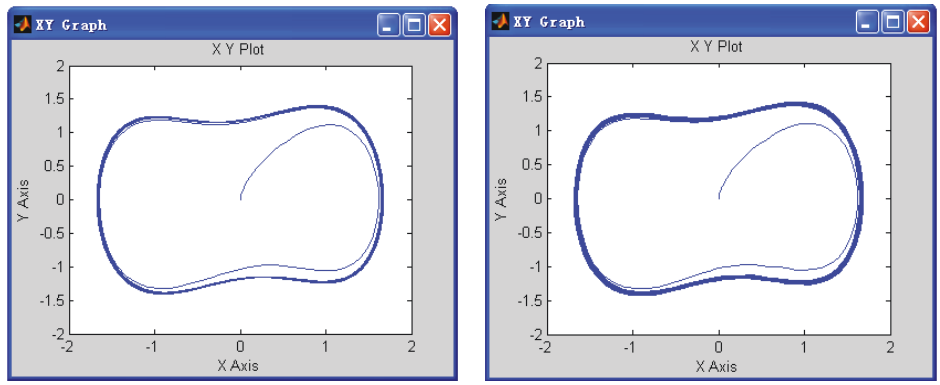

(a) No noise signal ($\gamma = 0.8261$) (b) Noise power = 0.1 mW ($\gamma = 0.8261$)

Figure 8: Duffing oscillator large-scale periodic state phase trajectory diagram.

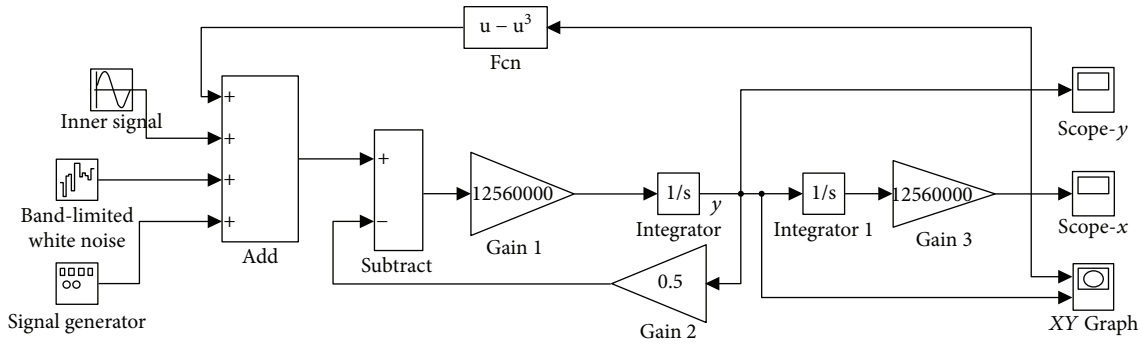

Figure 9: The improved duffing oscillator schematic diagram.

trajectory becomes coarse. For the signal amplitude of 10 mV, when the noise is increased to 2.8 mW, the system is no longer sensitive to the signal under test due to noise interference and the system is still in a chaotic state. With further simulation experiments, if the signal amplitude is 5 mV and the noise increased to 1.5 mW, the system appears chaotic and the SNR can reach −21 dB at the same time. For the same signal amplitude of 1 mV and the noise power which is increased to 0.33 mW, the system is still at a chaotic state and the SNR decreases to −28 dB.

The system sensitivity to the initial value demonstrates that the smaller the input signal amplitude, the more sensitive the system is to the signal, the better the system's antinoise performance, and the lower the signal-to-noise ratio. The simulation results show that the Duffing oscillator is sensitive to the signal under test and has good immunity to noise under certain background intensity noise. Therefore, the Duffing oscillator can be applied to detect weak electromagnetic logging signals.

4.2.2. Periodic State. Using the same Simulink numerical simulation model in Figure 6 and the same condition, damping ratio coefficient, $k = 0.5$, driving force signal frequency, $\omega = 1$ rad/s, initial values $(x(t), \dot{x}(t)) = (0, 0)$, the Duffing oscillator periodic state was analyzed. The generated signal under test had the same phase and frequency as the driving force. When there is no noise signal added and the driving force amplitude is $\gamma = 0.8261$, the system entered the periodic state and the phase trajectory diagram forms the smooth ring as shown in Figure 8(a). The addition of the white Gaussian noise with a noise power of 0.1 mW shows that the system is in the periodic phase state (Figure 8(b)). Comparing Figures 8(a) and 8(b), the phase trajectory diagram ring width limit increases and the boundary becomes rough as it is affected by noise signal perturbations. Simulation results show that the phase trajectory of the periodic state is relatively stable and the influence of noise on it is reasonably slight.

4.3. Improved Duffing Oscillator. The internal driving force signal under test having a response frequency of 2 MHz ($\omega = 12{,}560{,}000$ rad/s) and an amplitude of 1 μV was simulated using the MATLAB Simulink model shown in Figure 9 according to (16). The system damping coefficient was fixed at 0.5, the gain of gain 1 is equal to ω, the gain of gain 2 is equal to 0.5, and the gain of gain 3 is equal to ω at system initial values set to $(x(t), \dot{x}(t)) = (0, 0)$.

Before adding the noise signal, simulation results revealed that when the internal driving force signal amplitude reached 0.825306 V, the system entered the critical chaotic state and when the amplitude changed to 0.825307 V, the system entered the large-scale periodic state, as shown in

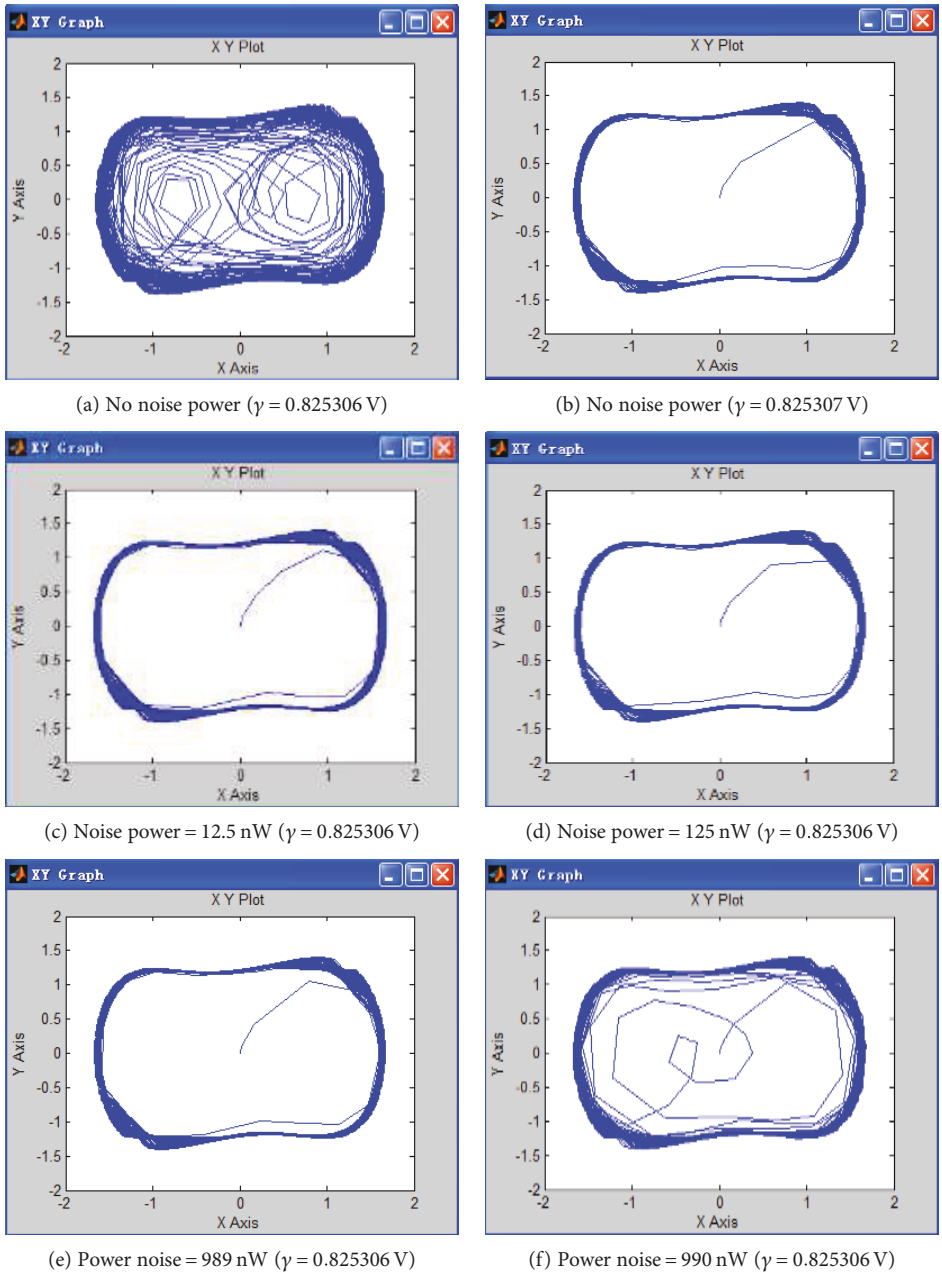

(a) No noise power ($\gamma = 0.825306$ V)

(b) No noise power ($\gamma = 0.825307$ V)

(c) Noise power = 12.5 nW ($\gamma = 0.825306$ V)

(d) Noise power = 125 nW ($\gamma = 0.825306$ V)

(e) Power noise = 989 nW ($\gamma = 0.825306$ V)

(f) Power noise = 990 nW ($\gamma = 0.825306$ V)

Figure 10: Diagram of the Duffing oscillator at a 2 MHz signal excitation phase state.

Figures 10(a) and 10(b), respectively. Under the same condition, the signal to be tested was added and the system performance measured at different noise power sources.

When the noise power of 12.5 nW, 125 nW, and 989 nW was added, the system was in a large-scale periodic state; however, when the noise power was increased to 990 nW, the system entered the chaotic state as shown in Figures 10(c)–10(f). These results showed that the Duffing oscillator system can detect the minimum signal-to-noise ratio (SNR) of at least −63 dB minimum power. These simulation results concluded that the improved Duffing oscillator system is sensitive to high-frequency signals and has good immunity to noise in the presence of the background noise intensity. Therefore, the Duffing oscillator can detect weak signals in response to the electromagnetic logging waves while drilling.

4.4. Circuit Simulation Results. From the Duffing oscillator circuit design of Figure 3, Multisim circuit simulation software was used to test the parameter design as shown in Figure 11. The nodes A and B correspond to x and y variables of the Duffing equation (20), while the virtual Multisim oscilloscope was used to monitor the phase trajectory characteristics in x-y planes.

The internal driving force is expressed by the signal source V2 set at a frequency of 2 MHz, and the signal source

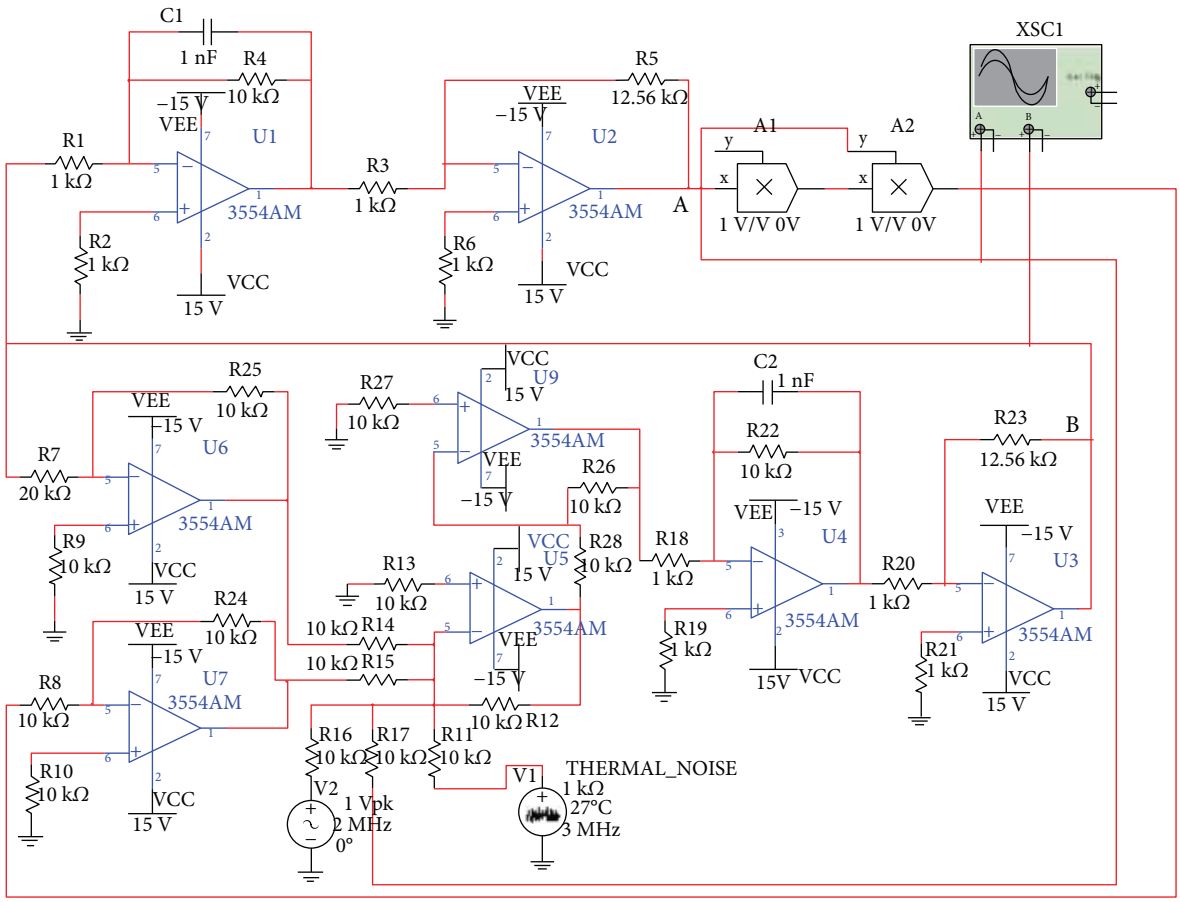

Figure 11: Duffing oscillator circuit.

voltage amplitude is continuously increased from 0. The oscilloscope shows that the system phase trajectory changes sequentially from the homoclinic state, chaotic state, and critical chaotic state to the large-scale periodic state. The simulation results shown in Figure 12 disclosed that when the signal source voltage reaches 0.771713 V, the circuit is in a critical chaotic state (Figure 12(e)), and when the signal source voltage is increased by 1 μV to 0.771714 V, the circuit is in a large-scale periodic state (Figure 12(f)). From the circuit simulations, the designed Duffing oscillator circuit has shown optimistic performance in detecting weak signals at high frequencies and is sensitive to the system initial values set in simulation settings.

5. Summary Discussions

The Duffing oscillator system phase trajectory diagram can sequentially evolve into noticeable nonlinear dynamic characteristics. The four phase states generated are the homoclinic orbit state, bifurcation state, chaotic state, and the evolution of the large-scale periodic state of the outer orbit state. In the critical state, small amplitude changes of the signal under test cause the phase locus to enter the large-scale periodic state from the chaotic state. When the system is in a critical state, the addition of the weak signal is certainly detected and recognized by discriminating the system phase state.

The Duffing oscillator is very sensitive to the additional of noise signals of different noise powers demonstrated by system phase states. The greater the noise intensity is, the more disorder the phase trajectory diagram has and the more the system enters into the chaotic state. Simulation results of different system chaotic depths have identified that the system antinoise performance relates to the magnitude of the driving force amplitude, γ. The closer the amplitude of the driving force is to the system critical state value, the better the antinoise performance sensitive to the systems. The appropriate selection of the driving force threshold value can make the Duffing oscillator system achieve reliable detection of weak periodic signals in certain noise intensity.

The effects of the damping ratio coefficient to the signal under test on the system antinoise performance principle of dynamic disturbance have demonstrated that the disturbance of the driving force signal is stronger than that of the damping ratio coefficient. To affect the output of the system, the driving force disturbance noise needs to be integrated twice while the damping coefficient ratio noise occurs after the first integration. From the tested signal simulations, the use of the dynamic disturbance mode of the driving force requires more stringent requirements than the use of damping ratios. For the dynamic disturbance mode, the signal under test and

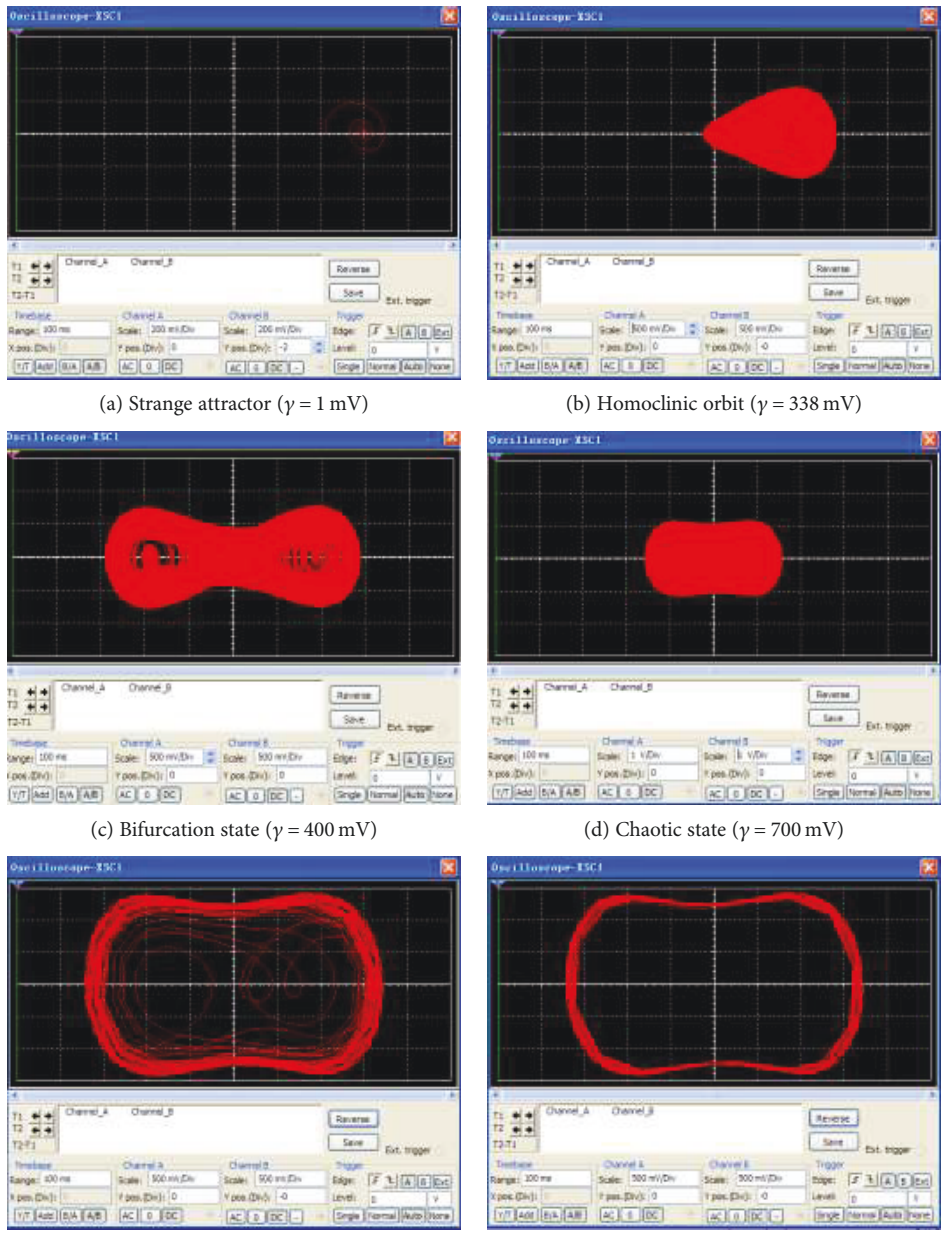

(a) Strange attractor ($\gamma = 1$ mV)

(b) Homoclinic orbit ($\gamma = 338$ mV)

(c) Bifurcation state ($\gamma = 400$ mV)

(d) Chaotic state ($\gamma = 700$ mV)

(e) Critical chaotic state ($\gamma = 771.713$ mV)

(f) Large-scale periodic state ($\gamma = 771.7134$ mV)

Figure 12: Simulated Duffing oscillator circuit phase state.

the internal driving force signal must be in phase and have the same frequency. However, the damping coefficient disturbance mode is created by the system's inherent perturbation characteristics and not constrained by the system's signal frequency and phase.

The improved Duffing circuit designed in Figure 3 was simulated using Multisim circuit simulation software to test the parameter design of Figure 11 on the signal under test detection performance in the presence of noise signals generated by the thermal noise equation. Thermal noise values were calculated from the equation, $P = 4kTRB$, where k is the Boltzmann constant (1.38×10^{-23} J/K), T is the resistance absolute temperature (K), R is the resistance value (Ω), and B is the noise bandwidth (Hz) of the measurement system. When selecting the thermal noise module, V1 was selected from the THERMAL_NOISE node located in Multisim's device library SIGNAL_VOLTAGE, and the values of resistance, R, temperature, T, and noise bandwidth, B, to determine thermal noise power were set and tested. Under certain set bandwidth and temperature values, varying the resistance, R, value will change the noise power values. The signal under test was measured by the AC voltage signal source, AC_VOLTAGE node, selected from the Multisim's device library SIGNAL_VOLTAGE_SOURCE. The system signal frequency was set to 2 MHz and the amplitude to 10^{-n} V, where n is the minimum unit of the critical value with regard to the driving force critical power accuracy. If the critical value is 0.77171 V, then the input signal under test

is 10 μV, and if the critical value is 0.771713 V, the signal changes to 1 μV.

During weak signal detection performance test, first, the signal source V2 amplitude was adjusted to observe the oscilloscope phase state if it matches the critical threshold value, and the Duffing circuit showed the chaotic critical state. The signal source amplitude, V2, was reset by subtracting the amplitude of the signal threshold value from the test signal amplitude, and then add the thermal noise V1 and later gradually increase the thermal noise power by increasing the resistance, R. As the critical threshold accuracy increases, the detectable signal-to-noise ratio (SNR) decreases. From the circuit simulation, the Duffing oscillator is sensitive to the initial value, and the weaker the signal, the more sensitive the Duffing circuit is to the signal and the stronger the antinoise performance.

6. Conclusions

The Duffing oscillator has good noise immunity performance to randomly distributed noise and is very sensitive to the initial signal under test values. Simulation results have shown that the Duffing oscillator system is sensitive to small amplitude changes of the input tested signal and has reasonable system antinoise performance to even lower signal-to-noise ratio (SNR) values. The influence of noise signal strengths on the Duffing oscillator generates noticeable nonlinear dynamic characteristics of phase trajectory locus states related to the noise intensity which affects the performance of system detection. Gradually, increasing the internal driving power and signal noise strengths causes the system to sequentially evolve into the homoclinic orbit state, bifurcation state, chaotic state, and the large-scale periodic state subject to the noise power strength applied. The greater the noise intensity, the more disorder the phase trajectory diagram has and the more the system enters into a chaotic state. The conventional Duffing oscillator has a weak detection system due to its lowest detection threshold nature. The designed improved Duffing oscillator circuit model has improved the detection threshold value and advanced the detection system performances. Simulation results on 2 MHz electromagnetic logging signal frequency demonstrated the system to be very sensitive to the random noise and high degree of noise immunity performance within the tested parameters and values. The critical threshold accuracy is improved, and the signal-to-noise ratio is reduced.

As the critical threshold accuracy increases, the detectable signal-to-noise ratio (SNR) decreases. The weaker the signal under test, the more sensitive the Duffing circuit is to the signal and the stronger the antinoise performance. Simulation results of different system chaotic depths have disclosed that the system antinoise performance relates to the magnitude of the driving force amplitude. The appropriate selection of the driving force threshold value can make the system achieve weak periodic signal detection in certain noise intensity. The output antinoise performance principle of dynamic disturbance is strongly affected by the driving force amplitude than by the damping ratio coefficient to the signal under test. From the tested signal simulations, the use of the driving force dynamic disturbance mode is more stringent than the use of damping ratios. Nevertheless, the signal under test and the internal driving force signal must be in phase and have the same frequency, but the damping coefficient disturbance mode is created by the system's inherent perturbation characteristics and not constrained by the system's signal frequency and phase.

Data Availability

The data used to support the findings of this study are included within this article or are available from the corresponding author upon request.

Conflicts of Interest

The authors declare that they have no conflicts of interest.

Acknowledgments

This work has been funded by the National Natural Science Foundation of China (nos. 51604038 and 51541408); the Laboratory for Marine Geology (no. MGQNLMKF201705) and Wenhai Program (no. 2017WHZZB0401) of Qingdao National Laboratory for Marine Science and Technology (QNLM); the Research Fund for the Taishan Scholar Project of Shandong Province (no. TSPD20161007); and the Department of Education, Hubei Province (no. D20141303).

References

[1] A. Hartmann, O. Akimov, S. Morris, and C. Fulda, "Improving real-time image-data quality with a telemetry model," *SPE Drilling and Completion*, vol. 27, no. 3, pp. 383–392, 2012.

[2] X. Liu, L. Bo, and Y. YUE, "Transmission behavior of mud-pressure pulse along well bore," *Journal of Hydrodynamics, Series B*, vol. 19, no. 2, pp. 236–240, 2007.

[3] C. Klotz, I. Wassermann, and D. Hahn, "Highly flexible mud-pulse telemetry: a new system," in *SPE Indian Oil and Gas Technical Conference and Exhibition*, Mumbai, India, March 2008.

[4] E. S. Shearer, "Pulse signaling for downhole telemetry," US 2010/0188253 A1, 2013.

[5] B.-N. Yan, C.-X. Liu, J.-K. Ni, and L. Zhao, "Demodulation of acoustic telemetry binary phase shift keying signal based on high-order Duffing system," *Chinese Physics B*, vol. 25, no. 10, article 100502, 2016.

[6] J. Zhao, W. Liyan, L. Fan, and L. Yanlei, "An effective approach for the noise removal of mud pulse telemetry system," in *2007 8th International Conference on Electronic Measurement and Instruments*, pp. 1–971, Xi'an, China, August 2007.

[7] A. Mollakhorshidi and R. Arabjamaloei, "Estimation of formation damage in overbalanced drilling using artificial neural networks and developing a simple correlation," *OIL GAS European Magazine*, vol. 42, no. 2, pp. 95–97, 2016.

[8] M. A. Namuq, M. Reich, and S. Bernstein, "Continuous wavelet transformation: a novel approach for better detection of mud pulses," *Journal of Petroleum Science and Engineering*, vol. 110, pp. 232–242, 2013.

[9] M. L. Psiaki, B. W, J. A. B. O'Hanlon, D. P. Shepard, and T. E. Humphreys, "GPS spoofing detection via dual-receiver

correlation of military signals," *IEEE Transactions on Aerospace and Electronic Systems*, vol. 49, no. 4, pp. 2250–2267, 2013.

[10] T. Barszcz and R. B. Randall, "Application of spectral kurtosis for detection of a tooth crack in the planetary gear of a wind turbine," *Mechanical Systems and Signal Processing*, vol. 23, no. 4, pp. 1352–1365, 2009.

[11] K. Shin, "Realization of the real-time time domain averaging method using the Kalman filter," *International Journal of Precision Engineering and Manufacturing*, vol. 12, no. 3, pp. 413–418, 2011.

[12] J. Wang, Q. He, and F. Kong, "Adaptive multiscale noise tuning stochastic resonance for health diagnosis of rolling element bearings," *IEEE Transactions on Instrumentation and Measurement*, vol. 64, no. 2, pp. 564–577, 2015.

[13] F. Bouaziz, D. Boutana, and M. Benidir, "Multiresolution wavelet-based QRS complex detection algorithm suited to several abnormal morphologies," *IET Signal Processing*, vol. 8, no. 7, pp. 774–782, 2014.

[14] G. Campetelli, D. Zumoffen, and M. Basualdo, "Improvements on noninvasive blood glucose biosensors using wavelets for quick fault detection," *Journal of Sensors*, vol. 2011, Article ID 368015, 11 pages, 2011.

[15] K. M. Hock, "Narrowband weak signal detection by higher order spectrum," *IEEE Transactions on Signal Processing*, vol. 44, no. 4, pp. 874–879, 1996.

[16] A. Tesei and C. Regazzoni, "Signal detection in non-Gaussian noise by a kurtosis based probability density function model," *In Practice*, vol. 1, p. 1, 1995.

[17] J. Yan and L. Lu, "Improved Hilbert–Huang transform based weak signal detection methodology and its application on incipient fault diagnosis and ECG signal analysis," *Signal Processing*, vol. 98, pp. 74–87, 2014.

[18] M. K. Ahirwal, A. Kumar, G. K. Singh, and J. S. Suri, "Sub-band classification of decomposed single event-related potential co-variants for multi-class brain–computer interface: a qualitative and quantitative approach," *IET Science, Measurement & Technology*, vol. 10, no. 4, pp. 355–363, 2016.

[19] S. A. Kassam, "Signal detection in non-Gaussian noise," in *Springer Science & Business Media*, Springer, New York, NY, USA, 1988.

[20] I. Song, J. Bae, and S. Y. Kim, "Advanced theory of signal detection," in *Signals and Communication Technology*, Springer, Berlin, Heidelberg, 2002.